Journal of Applied Polymer Science

Preparation and Characterization of Supported Ordered Nanoporous Carbon Membranes for Gas Separation

Bing Zhang,[1,2] Yi Shi,[1] Yonghong Wu,[1] Tonghua Wang,[2] Jieshan Qiu[2]

[1]School of Petrochemical Engineering, Shenyang University of Technology, Liaoyang 111003, China

[2]School of Chemical Egineering, Carbon Research Laboratory, State Key Laboratory of Fine Chemicals, Dalian University of Technology, Dalian 116024, China

Correspondence to: B. Zhang (E-mail: bzhangdut@163.com or zhangbing@sut.edu.cn)

ABSTRACT: Supported ordered nanoporous carbon membranes (ONCM) were prepared by coating a membrane-forming solution of resorcinol-formaldehyde (RF) resin on plate support through solvent evaporation and pyrolysis. The membrane solution was formed by the organic-organic assembly of RF resin with Pluronic F127 in the presence of triethyl orthoacetate and catalyst hydrochloric acid. The thermal stability of precursor, the microstructure, functional groups, and morphology and porous structure of resultant support and ONCM were investigated by the techniques of thermogravimetry, X-ray diffraction, Fourier transformed infrared spectroscopy, scanning electron microscopy/transmission electron microscopy and nitrogen adsorption-desorption, respectively. Results have shown that the as-obtained ONCM has well-developed porous regularity with bi-modal narrow pore size distribution. ONCM is tightly adhered to the adopted phenolic resin-based carbon support. Gases permeating through the ONCM are dominated by molecular sieving mechanism. The ideal gas separation factor of the supported ONCM can be reached to 46.4, 4.7 and 3.3 for H_2/N_2, CO_2/N_2 and O_2/N_2, respectively. The supported ONCM obtained in this work exhibits most promising application for permanent gas separation. © 2013 Wiley Periodicals, Inc. J. Appl. Polym. Sci. **2014**, *131*, 39925.

KEYWORDS: membranes; self-assembly; separation techniques; porous materials; gas

Received 15 June 2013; accepted 2 September 2013

DOI: 10.1002/app.39925

INTRODUCTION

Nanoporous carbon membrane (NCM) is a new type of porous inorganic membrane material, which is usually prepared by the pyrolysis of carbonaceous materials. Compared with traditional organic membranes, NCM has the advantages of anti-corrosion, solvent resistance, thermal stability, and excellent separation performance. At microcosmic level, NCM is consisted by enormous superfine nanoporous structure. Because the porous passages in this nanoporous structure are comparable to the kinetic diameters of gases, NCM can efficiently distinguish and separate desired molecules from gas mixture depending on molecular sieving or selective adsorption mechanism. Therefore, NCM has outstanding permeability and selectivity simultaneously and is much promising in gas separation fields.[1,2]

The original research work of NCM can be dated back up to 1960s. At that time, the main work is focused on the surface adsorption and diffusion process of gases passing through NCM.[3] Only in the early 1980s, the significance of NCM research has been gradually realized when Koresh and Soffer successfully fabricated defect-free hollow fiber carbon membranes with the best O_2/N_2 separation factor above 8.0.[4] During the last two decades, the rapid advances of NCM research have come out numerous significant works. On the whole, those works can be divided into three aspect, aiming at improving separation performance: (1) Optimization of preparation protocols and pyrolysis condition;[1,2] (2) Development or modification of carbon precursors, e.g., hybridization;[5–7] (3) Design of novel structure in NCM, e.g., honeycomb-like porous structure.[8,9] In addition, Wang et al.[10] invented spiral wound NCM with large loading amount. Kimijima et al.[11] developed NCM with ordered channel structure. Anderson et al.[12] utilized positron annihilation lifetime spectroscopy technique to characterize the porous structure of NCM. All those works have overwhelmingly promoted the advancement of NCM and brought people with more confidence for future potential application. Before practical application, some urgent problems have to be solved for NCM, including high-cost and fragility.[13] The fragility of NCM are usually conquered by adhering to robust porous support with the help of various complicated coating techniques.[1,2] The high-cost has to be saved by reducing fabrication process or compensated by improving separation performance.

Among the newly developed carbon membrane materials, researchers have previously found that carbon membranes with

ordered porous structure, or so-called ordered nanoporous carbon membranes (ONCM), would have super high flux and selectivity for the separation of gas (or liquid) mixture by experimental and theoretical analysis.[14–18] The reason is that ONCM can provide unmatched molecular sieving ability and reduced diffusion resistance for gas mixture than traditional NCM (with amorphous worm-like structure). However, up to date, only few reports have referred to the gas separation performance of ONCM, to our best knowledge. One reason is the occurrence of shrinkage parallel to the membrane-forming substrate during solidification and heat treatment, leading to the fabrication of large-sized ONCM being more difficult than its other analogue forms, such as powder and monolith.[19] Liang et al.[20] used the assembly of resorcinol-di-block copolymer mixture to fabricate an ordered nanoporous carbon film through the processes of solvent treatment, polymerization with formaldehyde and pyrolysis at 800°C. Zhao's group[21,22] obtained free-standing ordered nanoporous carbon films through the pyrolysis of an assembly composite formed by phenolic resin and a cheap tri-block copolymer (PEO-PPO-PEO). Simanjuntak et al.[23] utilized 1,5-dihydroxynaphthalene to prepare ordered nanoporous carbon film with well-ordered hexagonal channel-like porous structure. Tanaka et al.[24] also obtained ordered nanoporous carbon film from resorcinol–phloroglucinol/formaldehyde polymer and triblock copolymer Pluronic F127 by dip-coating method. We can see that nearly all the above-mentioned reports refer to "ordered nanoporous film" instead of "ordered nanoporous membrane" because the most obtained films are merely in the form of fragments that could not be anticipant of fulfilling any separation task in practice. Therefore, the fabrication of large-sized ONCM has become one challenge for researchers. Until now, only Kimijima et al.[11] have reported an ONCM having the gas separation ability within the domination of Knudsen diffusion, which was prepared by coating on the surface of porous anodic alumina through the processes of drying and pyrolysis. To further pursue more satisfactory gas separation performance, here we attempted to fabricate supported ONCM for gas separation application by the assembly of organic-organic molecules on the surface of plate support.

EXPERIMENTAL

Materials

The raw materials of support were commercially obtained, including phenolic resin (industrial grade), methyl cellulose (industrial grade) and hexamethylene tetramine (analytical grade, AR). The starting materials of ONCM is composed by resorcinol (abbreviated as R, AR, Tianjin Damao Chemical Reagent Factory), formaldehyde (or formalin, abbreviated as F, 38% in water), triethyl orthoacetate (EOA) (AR, Alfa Aesar) and ethylene oxide/propylene oxide block copolymer Sigma-Pluronic F127 ($EO_{106}PO_{70}EO_{106}$). In addition, ethanol (AR, 98% in weight percentage) and hydrochloric acid (38% in volume percentage) were adopted as solvent and catalyst, respectively. During the measurement of macroporous pore size distribution of support, isopropyl alcohol with analytical grade was used as wetter.

Preparation of Ordered Nanoporous Carbon Membrane

In this work, two kinds of ONCM, i.e., free-standing ONCM and supported ONCM, were fabricated for convenience. Free-standing ONCM was first formed in order to eliminate the possible disturbance of support on the textural characterization of ONCM samples.

Free-Standing ONCM

First, a resorcinol solution was prepared by dissolving 1.65 g resorcinol into 4.35 g distilled water, followed by putting into 5.75 g ethanol, 0.27g hydrochloric acid and 0.945g template F127, under vigorous stirring in 30°C water bath. At the same time, another formaldehyde solution was also formed by dissolving 1.2 g EOA into formalin. The motivation for us to use EOA is due to the suggestion that small molecules EOA can effectively reduce the polymerization rate of R with F during assembly by promoting the formation of organic–organic network structure, as well as thermal stability and char yield.[19] Assembly process along with the polymerization of R-F was performed by adding the latter F solution into the former R solution by vigorous stirring for 20–30 min. Consequently, an RF membrane-forming solution was obtained. Free-standing polymeric membrane was fabricated by pouring the membrane-solution onto the surface of a sanitary horizontal glass plate through drying and membrane solidification. The temperature program for drying was set at 30°C for 24 h and 100°C for 24 h, to ensure the complete solvent-evaporation and solidification. RF membrane samples were ultimately obtained by scraping the polymeric membranes from the glass plate with a knife. Figure 1 shows the schematic polymerization process of RF and the formation of assembly structure with F127, referenced from the literature report.[25]

ONCM samples were obtained by the direct pyrolysis of polymeric membranes loaded in crucibles at a horizontal furnace with a programmable temperature controller. The pyrolysis program was first set from ambient temperature to 400°C at a heating rate of 2°C/min. After holding at 400°C for 3 h, it was ramped to 600°C at 1°C/min and holding for 6 h at 600°C before cooling down to room temperature. Inert atmosphere was kept by 100 mL/min highly purified nitrogen streaming throughout the pyrolysis.

Supported ONCM

The preparation process of supported ONCM contains two steps: support fabrication and coating formation.

The fabrication of plate support undergoes three stages: dough, mould and pyrolysis. First, phenolic resin powder (30 g) was partially cured with 3.6 g hexamethylene tetramine at 150°C for 1 h, followed by grinding into powder until the mean particle size around 0.2−0.3 μm. A damp-dry mixture was obtained by mechanical agitating the above-formed phenolic resin powder with 3.6 g methyl cellulose and suitable water for 1 h. Dough was formed after kneading and aging the damp-dry mixture for 80 min. The dough was pressed in a mould to shape plate circular with the diameter of 3 cm and thickness of 5 mm. To avoid suncrack, the nascent support samples were kept out of the sun for 2−3 days to naturally remove the remaining solvent for further use as support. The final pyrolysis was usually conducted after coating process except for textural characterization.

The coating process was performed by two methods, immersing (dipping) support into membrane-forming solution for 2–60 s

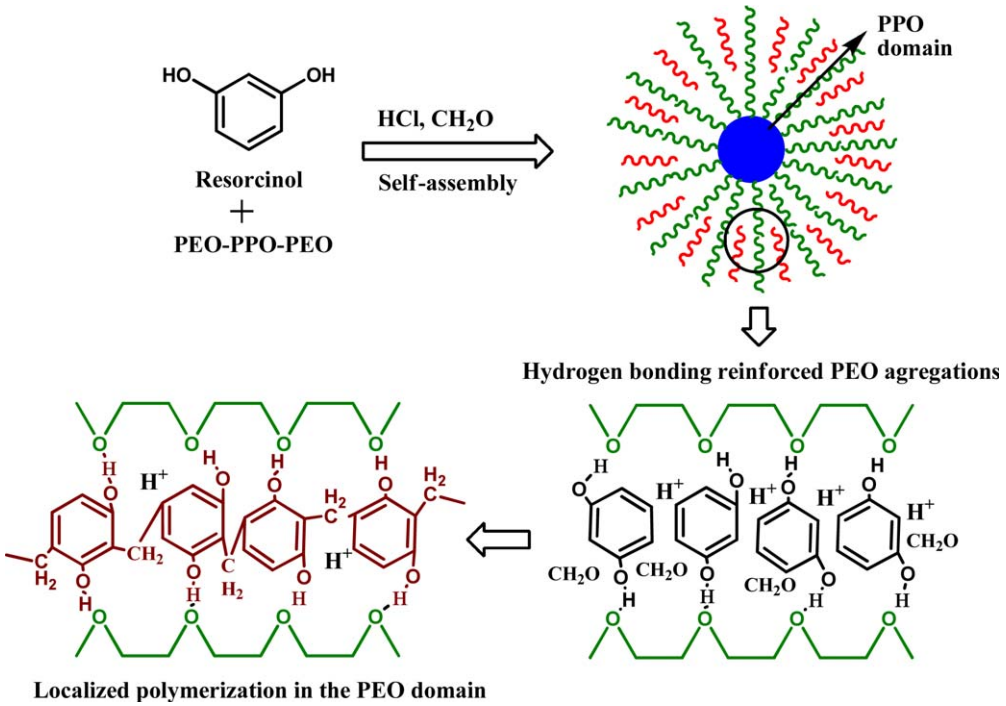

Figure 1. Schematic of the polymerization reaction of resorcinol-formaldehyde and the formation of assembly structure with F127. [Color figure can be viewed in the online issue, which is available at wileyonlinelibrary.com.]

by one time, or dropping solution onto the support surface by many times. Then, the wetty coated support was dried at 30°C for 24 h and 100°C for 24 h. The subsequent pyrolysis protocol was adopted by the same condition as the above-mentioned free-standing ONCM. The final samples were denoted as ONCM-Ime (x) s and ONCM-drp (y), reflecting the two coating method, i.e., immersing by x seconds and dropping by y droplets, respectively.

Characterization

The thermal stability of precursors for ONCM and support was characterized by a TGA851^e Mettler Thermo-gravimetric analyzer at a heating rate of 10°C/min from ambient temperature to 900°C under flowing nitrogen.

The average particulate dimension of ground phenolic resin powder was measured with a DLS particle size analyzer (Model: ZEN3690, Malvern Instruments Ltd., UK).

The surface morphology of supported ONCM was observed by a TM-3000 scanning electron microscopy (SEM) (Hitachi) at an accelerating voltage of 15 kV on a standard observation mode. In addition, a JEM-2100 transmission electron microscopy (TEM) (JEOL) was also used in order to further insight into the microstructural texture of ONCM samples.

The carbon structure of ONCM support was analyzed by a D/max2500 X-ray diffraction analyzer (Rigaku) in the 2θ range of 5–60°, at the operation of 40 kV and 80 mA.

The functional groups in precursor were monitored by a Nexus 470 attenuated total reflectance- Fourier transform infrared spectroscopy (ATR-FTIR, Thermo Nicolet) with a OMNIC software in the wavenumber range of 4000–680 cm^{-1}.

Pore size distribution for macropores of pyrolyzed support was characterized by a soap bubble method using isopropyl alcohol as wetter for its low surface tension.[26] The porosity was measured by the criterion method of China National Standards GB/T 1966–1996.[27]

The pore size distribution of mesopores and micropores for pyrolyzed support and ONCM layer were measured by an ASAP 2420 nitrogen adsorption analyzer (Micromeritics, USA) at −196°C. Ahead of measurement, all ONCM samples were degassed at 300°C for at least 6 h.

Measurement of Gas Permeance

Pure gas permeability of ONCM for H_2, CO_2, O_2, and N_2 was tested by conventional variable volume-constant pressure method. The highly purified gases (≥99.999%) directly supplied from gas cylinders are fed to the upper side of membrane cell, in which carbon membranes were sealed by epoxy glue and O-shaped gasket. Although the supported ONCM can easily tolerate high pressure up to 0.5 MPa, we usually conducted the gas permeation test at 0.2 MPa due to the safety consideration. The pressure of permeating side was kept at ambient atmosphere. The permeating temperature of gases across carbon membranes was maintained at 25°C. The flux of permeating gas was measured by a micro-flowmeter. Single gas permeability was calculated by eq. (1).

$$P_i = {}^{F \cdot l}/_{A \cdot \Delta P} \quad (1)$$

where P_i is the permeability (1 Barrer = 10^{-10} cm^3 (STP) cm/cm^2 s cm Hg = 7.5×10^{-18} m^2 s^{-1} Pa^{-1}) of gas specie i; F is the gas flux permeating through the membrane; A and l are the effective membrane area and membrane thickness, respectively;

ΔP is the pressure difference between the feed side and the permeating side.

The ideal selectivity of gas pairs was obtained by the ratio of the permeability of two tested gases (e.g., O_2 and N_2) as shown in eq. (2).

$$S_{O_2/N_2} = {}^{P_{O_2}}/_{P_{N_2}} \quad (2)$$

The permeability of each gas permeating through ONCM sample was measured at least three times to ensure good precision and accuracy. The detailed procedure can also be found in our previous report.[28]

RESULTS AND DISCUSSION

Characterization of Support

Free-standing ONCM is unsuitable for practical application owing for its low mechanics in nature. If ONCM is supported by a robust support, the membrane-forming and mechanical properties would be undoubtedly improved significantly. Moreover, it would also be beneficial to reduce the effective thickness of ONCM layer and the diffusion resistance of permeating gases, resulting into the improvement of gas permeation.[29] In this work, plate phenolic resin-based support was utilized as support to prepare supported ONCM because of its close property to the starting material of ONCM. We believe that the support will surely provide tight affinity force to the ONCM layer. Anyhow, it is necessary to first characterize the support as follows.

Thermal Stability of Precursor

Thermal stability of precursor is an important property for carbon material, which can provide us with the thermal degradation mechanism and the determination of pyrolysis protocol. Figure 2 shows the thermal weight losses and their rate curves of phenolic resin-based support. We can see that the thermal degradation of precursor can be divided into four stages: ~160°C, 160~330°C, 330~450°C, and 450~600°C. Minor weight loss happens to the precursor at the first stage (I) of thermal degradation. This is due to the removal of remaining solvent water and the release of some gases formed by further curing reactions of phenolic resin.[30] All the following three weight losses are substantial in the subsequent stages. Judging from the weight loss curve of methyl cellulose, we can notice that the main contribution of weight loss is ascribed to the degradation of methyl cellulose for the second temperature stage (II). While in the third stage (III, 330~450°C) and fourth stage (IV, 450~600°C), two strong shoulder peaks correspondingly appear around the peak positions of 395°C and 531°C in the weight loss rate curve. The reason for (III) stage is that the release of small pyrolytic fragments formed by the clearage of methylene bridged phenolic ring structure with some hydroxymethyl and methylene ether groups, oxymethylene species, and oxidation products of formaldehyde.[31] In (IV) stage, various large fragments will be evolved from the matrix with the breakage of the backbone.[32] When the pyrolysis temperature is up to 600°C, the thermal degradation curve becomes placid. The final char yield of phenolic resin-based support is 53.0% at the temperature of 900°C. The high thermal stability of the used support is very favorable to improve the mechanics of final composite carbon membranes. Therefore, phenolic resin is one of the most popular precursors to prepare carbon membranes as claimed in literature.[33]

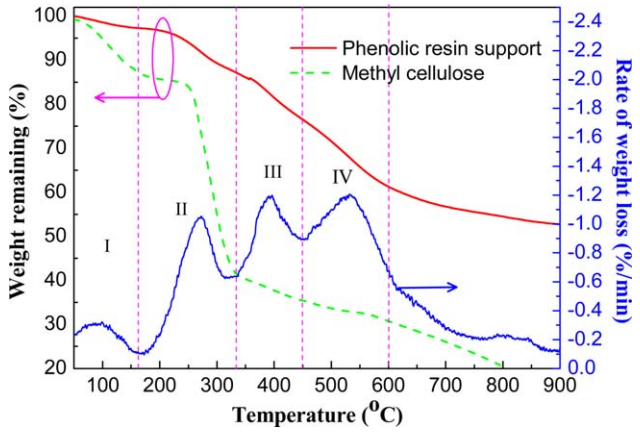

Figure 2. Thermal weight loss and their rate curves of phenolic resin support. [Color figure can be viewed in the online issue, which is available at wileyonlinelibrary.com.]

Microstructure and Pore Size Distribution

It is necessary to characterize the textural framework and porous structure of a support to evaluate its practical application. Figure 3 gives the XRD pattern of the pyrolyzed support. In XRD pattern, the (002) plane diffraction peak position locates around 20°. According to the well-known Bragg's equation, the interlayer distance d_{002} value is calculated as 0.443 nm that is much larger than the value of pure graphite (0.354 nm). It illustrates the low graphitization degree is for the pyrolyzed support. For amorphous carbon materials like the support in present work, low graphitization degree is usually expected to have high porosity, as will be discussed in the following.

Pore Size Distribution

The macro-pore size of the pyrolyzed support is distributed in the range of 0.05–0.3 μm with the peak position at 0.1 μm, as

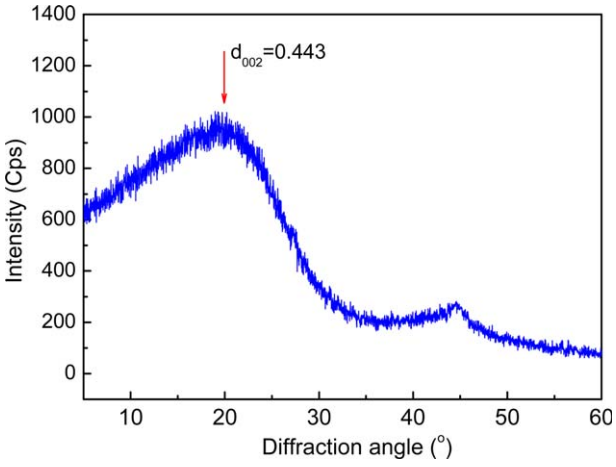

Figure 3. XRD pattern of pyrolyzed support made from phenolic resin. [Color figure can be viewed in the online issue, which is available at wileyonlinelibrary.com.]

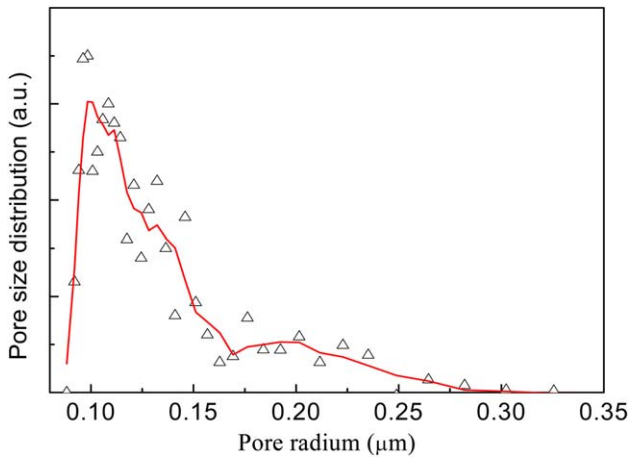

Figure 4. Macropore size distribution of pyrolyzed blank support made from phenolic resin. [Color figure can be viewed in the online issue, which is available at wileyonlinelibrary.com.]

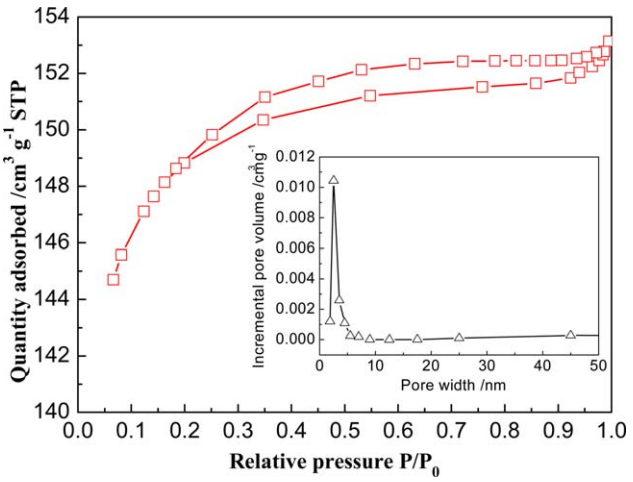

Figure 5. The adsorption–desorption curves and mesoporous and microporous pore size distribution of pyrolyzed blank support. [Color figure can be viewed in the online issue, which is available at wileyonlinelibrary.com.]

shown in Figure 4. Besides, the porosity of the pyrolyzed support is 40.1% calculated by the national standard test method. It demonstrates that the used support is rich in porous structure.

Although the macro-pore size distribution and porosity of the pyrolyzed support can be easily determined according to the above-mentioned practical methods, it is still incomplete to depict the full porous structure information due to the definite co-existence of some mesopores and micropores in the matrix. Hence, another important technique, nitrogen adsorption technique, was also applied to complementarily determine the porous parameters about the pyrolyzed support. The nitrogen adsorption-desorption curve, as well as its derived pore size distribution, of the pyrolyzed support are shown in Figure 5. With increasing the relative pressure, the adsorption amount of nitrogen successively elevates for support until up to the largest value of 153 cm^3/g at the final relative pressure of 1.0. A hysteresis loop is constructed by the curves of adsorption and desorption, illustrating that meso-porosity exist in the matrix. In addition, it can also be found that the narrow pore size distribution is centered at the peak position of 2 nm, as shown in the embedded images in Figure 5. Furthermore, some important porous parameters show the pyrolyzed support also containing plentiful porous structure listed in Table I, such as BET surface area (498.1 m^2/g), total pore volume (0.236 cm^3/g) and mean pore diameter (1.90 nm). From Table I, it can also be found that the pyrolyzed support is mainly composed by microporous structure along with a small amount of mesopores.

Combining the results of two pore size distributions from two techniques, it concludes that the support predominantly consists two kinds of porous dimensions: nanopores concentrated at 2 nm and macropores centered at 0.1 μm. It suggests that the formation of the two kinds of pores are due to the disordered stacking of amorphous carbon sheets and carbonaceous clusters, respectively, as will be further discussed in the later section of this article.

In sum, the present support is much attractive for production of supported membranes in view of the merit of cost-effective, easy fabrication, and fruitful porosity.

Ordered Nanoporous Carbon Membrane Layer

Thermal Stability of Precursor. Figure 6 shows the function of thermal degradation behavior of the precursor for ONCM with pyrolysis histories. In the whole temperature range two obvious thermal degradation stages can be found, i.e., (I) 200∼350°C and (II) 350∼420°C. Before 200°C, minor weight loss about 0.8% is mainly due to the evaporation of residual water and volatiles derived from the degradation of some oligomer and small molecules (e.g., EOA) during the (I) stage. In the (II) stage, 350–420°C, the weight loss about 41.9% is mainly contributed by the degradation of RF resin and di-block copolymer F127. Seen from the weight loss curve of F127, it can be found that the char yield is almost approaching to zero at 420°C, revealing that the F127 has been degraded completely at this temperature. As the pyrolysis temperature elevates further from 600°C, 800°C to 900°C, the weight loss curve gradually reaches to a plateau, with the char yield slightly reducing from 33.82%, 28.9% to 27.6%, respectively. Therefore, the present set pyrolysis temperature holding at 400°C and 600°C for a specific period

Table I. Pore Structure Parameters of Pyrolyzed Blank Support

Item	BET specific surface area/m^1/g	BJH mesopore volume (cm^3/g)	t-plot micropore volume (cm^3/g)	Total pore volume (cm^3/g)	Mean pore diameter (nm)
Parameters	498.1	0.039	0.134	0.236	1.90

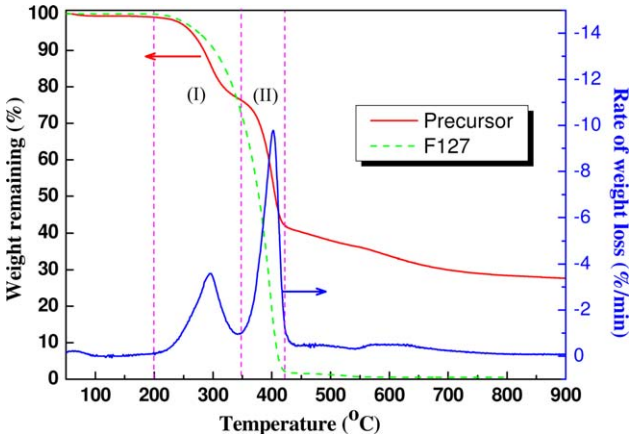

Figure 6. Thermal weight loss and its rate curves of RF-based precursor. [Color figure can be viewed in the online issue, which is available at wileyonlinelibrary.com.]

could assure the full degradation of F127, leading to the formation of final ordered porous carbon structure in ONCM.

ATR-FTIR Analysis. The ATR-FTIR analysis will help us to further understand the formation of assembly structure, as well as the final porous structure of ONCM. In Figure 7, typical reflectance peaks can be clearly found for precursor, such as the stretching vibrations of —C═C— double bond in aromatic rings (1610 cm^{-1}), C—O bond (1100 cm^{-1}), C—H bond (800–3000 cm^{-1}) and —OH bond (3600–3700 cm^{-1}). Among them, ether bonds during the scope of 1100–1400 cm^{-1} are due to the conjunct contribution of the existence of C—O—C structure in RF resin, EOA, and F127. In precursor, resorcinol has two functions: One is to react with formaldehyde by forming RF resin and further to evolve into the backbone of final ONCM; the other is to develop self-assembly structure with F127 by forming stable three-dimensional network structure. The latter structure is the rudimental framework of ultimate ordered porous structure in ONCM. Among the two reactions, the organic–organic

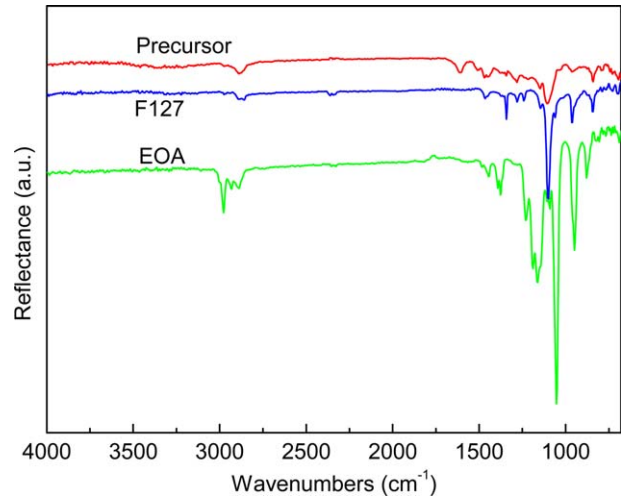

Figure 7. Fourier transformed infrared spectra of samples. [Color figure can be viewed in the online issue, which is available at wileyonlinelibrary.com.]

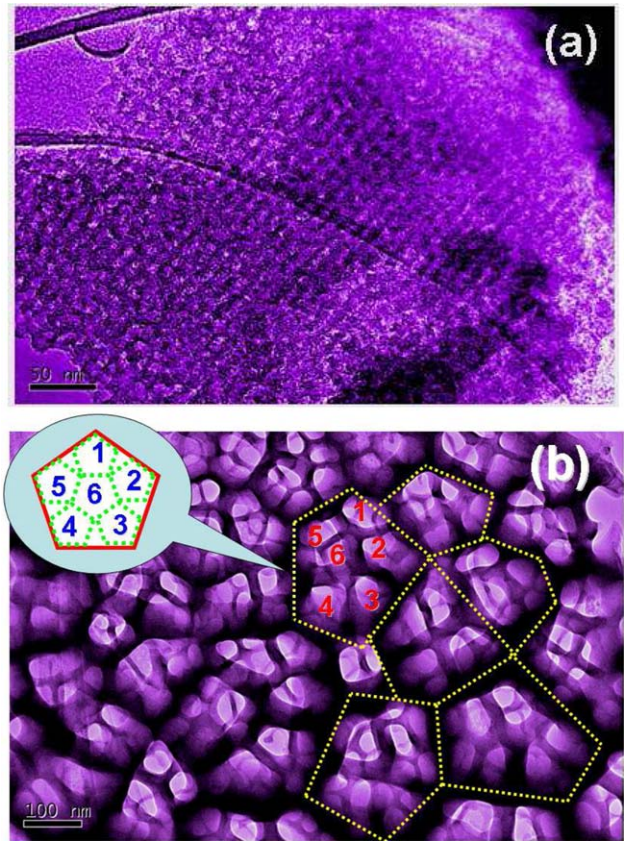

Figure 8. TEM images of free-standing ONCM. (a) General porous structure, and (b) local three-dimensional porous structure. [Color figure can be viewed in the online issue, which is available at wileyonlinelibrary.com.]

assembly would preferentially happen owing to the interaction of resorcinol with F127 being stronger than that with formaldehyde. It is believed that the two reactions are very fast under hydrochloric acid. The presence of EOA can effectively reduce the reaction rate of polymerization and crosslinking reactions. This is significant for the formation of network structure and ordered nanoporous structure.[19] In all, we are confident that the present constitution of precursor can successfully produce ONCM.

Morphology Observation. In the TEM image [Figure 8(a)], we can see that large amount of parallel black strips alternates with white strips that are the reflection of ordered porous channels in carbon matrix. According to the scalar bar, the channel width of the present ONCM is about 11nm that is close to the value of 8 nm as reported by Kimijima et al.[11] However, they did not provide any high resolution TEM except SEM images in that article. It is also notably found that a stereo-structure exists in some local region as shown in Figure 8(b), one larger quasi-pentagonal pore containing six smaller quasi-pentagonal pores. The six small pores were correspondingly occupied the five angles and center. This is much different from any other ordered porous carbon materials in literature, which is commonly a similar stereo-structure with oval or hexagonal shape.[34] It is speculated that the larger pores about 100 nm in width is

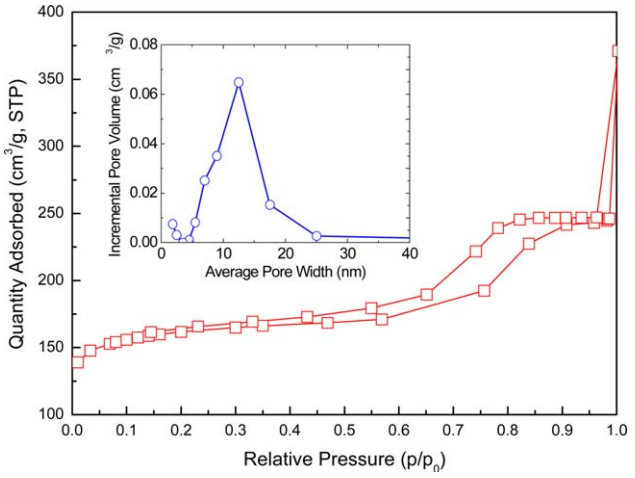

Figure 9. Nitrogen adsorption–desorption isotherms and pore size distribution curves of free-standing ONCM. [Color figure can be viewed in the online issue, which is available at wileyonlinelibrary.com.]

directly originated from the pyrolysis of the backbone of RF resin. While the smaller pores is from the assembly structure induced by F127. Taking a close look at the detailed structure, some blurred thin film layers could be identified as a cover function for the opening of every porous channel. This may be the evidence for the modification of porous structure by excessive amorphous carbon. As the result, the modified ONCM would exhibit better gas separation performance although the apparent pore size is too large to effectively separate gas mixture.

Adsorption Isotherm and Pore Size Distribution. Nitrogen adsorption technique is a most popular and powerful tool to gain the porous structure information of carbon materials. Figure 9 shows the nitrogen adsorption–desorption isotherm and pore size distribution of ONCM. The isotherm is strictly conformed to the typical type-IV curve according to the classification of IUPAC.[35] In isotherm, steep step occurs at $P/P_0 = 0.50$–0.80 associated with nitrogen filling of the mesopores owing to the capillary condensation. It indicates that the ONCM has uniform pore size, which is confirmed by the narrow pore size distribution curve (Figure 9 insert), centered at 12.43 nm. The pore size calculated from nitrogen adsorption is close to the value estimated from TEM images. The BET surface area and total pore volume of the ONCM are correspondingly 613 m^2/g and 0.38 cm^3/g as listed in Table II. Those values are comparable with literature report.[36,37] Furthermore, it can also be found that the ONCM prepared in the present work still has approaching values of mesoporous volume to microporous volume. As is well-known, such large pore diameter could not exert any separation function for gas mixture. As has discussed in the previous TEM section, the macro-pores may be modified by amorphous carbon sheets on the pore mouth. In fact, we can also found another half pore size distribution profile beneath 2 nm (Figure 9 insert), which is the reflection of micropores in ONCM. The half pore size distribution is obtained due to the limitation of the measurement of nitrogen adsorption technique. In addition, dead-end pores in sample would also contribute to the mean pore diameter value calculated by nitrogen adsorption–desorption isotherms. So the most effective indicator of pore structure for ONCM should have to be further investigated by gas permeating test.

Supported ONCM

Morphology Observation. The morphology of pyrolyzed support and supported ONCM was observed by SEM. From the pyrolyzed blank support [Figure 10(a)], we can see that the coarse surface is entirely composed by the random stacking of large amount of particles with varying diameters, leading to form abundant macroporous voids. It proofs well the previous analysis of pore size distribution in Figure 4. While for the supported ONCM sample ONCM-Drp11, the compact surface ONCM layer is defect-free as shown in Figure 10(b). It illustrates that the ONCM is well adhered to the support with good comparability. However, for the best composition result, it should be carefully controlled the coating process by the fine tuning of immersing time or droplets. Otherwise, the formed surface coating tends to be defective as shown in Figure 10(c–e).

Gas Permeance Test. The permeability and ideal selectivity of pure gases are listed in Table III. We can see that the nitrogen permeability is obviously reduced for ONCM prepared by coating, in comparison with blank pyrolyzed support. In addition, the nitrogen permeability of supported ONCM first decreases then increases with the immersing time elevating from 2 s to 60 s. The lowest value of 1.16 Barrer is obtained at the immersing time of 10 s. At the same time, the highest ideal selectivity is also reached. The gas permeability of nitrogen increases for ONCM obtained from drop-coating by three orders of magnitude with the coating droplets increasing from 11 drops to 19 drops.

It can be found that the gas separation performance of present ONCM-Ime10s, ONCM-Ime20s, and ONCM-drp11 is much higher than the Knudsen diffusion factor, i.e., 3.74 (H_2/N_2), 0.80 (CO_2/N_2), and 0.94 (O_2/N_2). We can also notice that the

Table II. Comparison of the Pore Parameters of Present Free-Standing ONCM with Other Ordered Mesoporous Carbon Materials in Literature

Sample	BET surface area (m^2/g)	BJH mesopore volume (cm^3/g)	t-plot micropore volume (cm^3/g)	Total porous volume (cm^3/g)	Mean porous diameter (nm)	Source
ONCM	613	0.172	0.190	0.38	12.4	This work
Ordered mesoporous carbon	602	–	–	0.43	4.7	Ref. 36
Ordered mesoporous carbon	398	–	–	0.32	3.9	Ref. 37
Ordered mesoporous carbon	763	–	–	0.64	3.3	Ref. 37

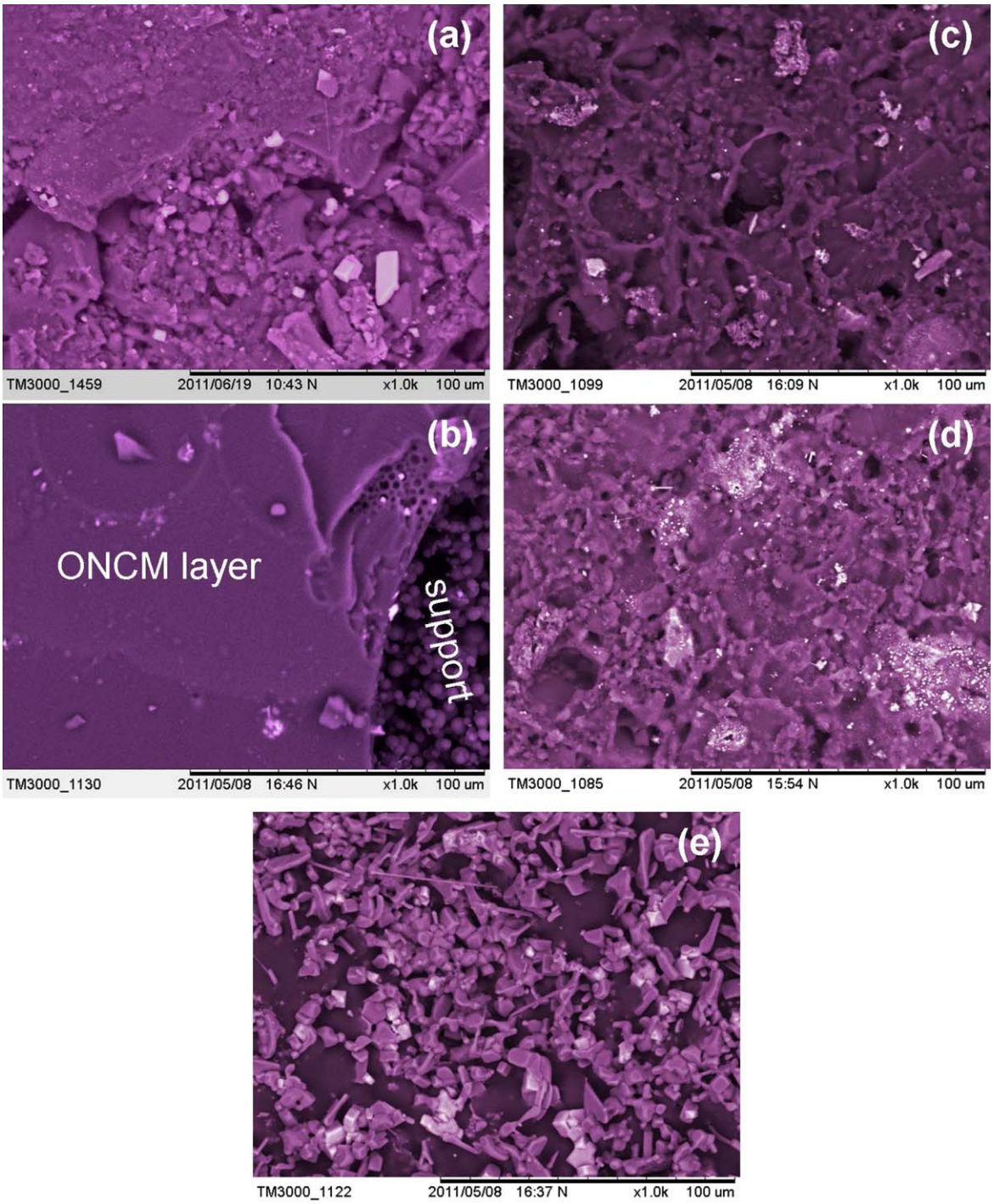

Figure 10. SEM images of pyrolyzed blank support (a), ONCM-drp11 (b), ONCM-drp5 (c), ONCM-Ime5s (d), ONCM-Ime60s (e). [Color figure can be viewed in the online issue, which is available at wileyonlinelibrary.com.]

gas permeability of the three ONCM samples follow the sequence of $H_2 > CO_2 > O_2 > N_2$, which is just in the reverse order of the kinetic diameter of gas molecules (H_2 (0.289 nm), CO_2 (0.33 nm), O_2 (0.346 nm), and N_2 (0.364 nm)). It suggests that gases permeating through the as-made supported ONCM are dominated by molecular sieving mechanism. However, the present gas separation performance seems to be against with the pore diameters of ONCM as previously detected around 11 nm from TEM and nitrogen adsorption techniques (Figure 9). Such large pore diameter should not exhibit any obvious separation factor for gases with the kinetic diameters beneath 0.4 nm, i.e., H_2, CO_2, O_2, and N_2. It can be interpreted by the modification of compact thin amorphous carbon film covering on the opening of pores. Besides, the pore size distribution calculated by the nitrogen adsorption–desorption isotherm actually contains the contribution of blind pores and fake pores. Considering

Table III. Gas Permeation Performance of Supported ONCM

	Permeability/barrer[a]				$S_{A/B}$		
Sample code	H_2[b]	CO_2	O_2	N_2	H_2/N_2	CO_2/N_2	O_2/N_2
Knudsen diffusion	-	-	-	-	3.74	0.80	0.94
Blank pyrolyzed support	-	-	-	2.5×10^6	-	-	-
ONCM-Ime2s	-	-	-	1.0×10^5	-	-	-
ONCM-Ime5s	-	-	-	1.9×10^4	-	-	-
ONCM-Ime10s	84.20	7.60	5.40	1.16	46.4	4.7	3.3
ONCM-Ime20s	205.62	17.67	14.21	9.03	16.2	1.4	1.1
ONCM-Ime40s	-	-	-	7.7×10^4	-	-	-
ONCM-Ime60s	-	-	-	1.2×10^6	-	-	-
ONCM-drp11	293.40	33.24	45.51	10.35	20.2	2.3	3.1
ONCM-drp19	-	-	-	4.9×10^4	-	-	-

[a] 1Barrer=1×10^{-10} cm^3 (STP) cm/cm^2 s cm Hg=7.5×10^{-5} cm^3 (STP) cm/cm^2 s kPa.
[b] The gas permeability of H_2 is tested under the pressure difference of 0.1 MPa.

this, it is not surprising to see the high separation performance of the present ONCM. When the dip-coating time prolongs from 10 s to 20 s (i.e., OCM-Ime10s and OCM-Ime20s), the permeability is improved by 2.5–8.5 times, along with the selectivity reducing by three times. Whereas, the separation performance could be entirely lost if the immersing time is too long or short, due to the defect formation in surface coating layer as shown in Figure 10(d,e). In the case of dropping protocol, the obtained ONCM-drp11 has both satisfactory permeability and selectivity overall. Likewise, the selective property would also be definitely lost if the number of droplets adopted were inappropriate during coating process as illustrated in Figure 10(c). The difference in best gas permeance of ONCM samples fabricated by the two protocols may be due to the solvent evaporation.[38] We believe that the repetitious dropping method makes the evaporation of solvent more even and slow, in comparison with the one-time dip-coating method. The former method tends to form denser ONCM by constructing an overlapped crosslinking network membrane layer as the result of repeated process of dropping-drying. It leads to the ultimate ONCM with outstanding gas separation performance.

Tanaka et al.[39] produced supported ONCM at the pyrolysis temperature of 600°C on the surface of alumina by adopting resorcinol/phloroglucinol/formaldehyde mixture as precursor. They judged that the obtained ONCM has the separation ability of Knudsen diffusion by the sole permeation test of gas N_2. In the present work the as-obtained supported ONCM exhibits most attractive molecular sieving performance for permanent gases. In this work, we first bring forth the promising for ONCM to separate gases in systematic experiment. It will inspire more attention for the control and modification of porous structure of ONCM by similar route for gas separation.

CONCLUSIONS

Supported ordered nanoporous carbon membrane (ONCM) was successfully prepared by coating an assembly solution of resorcinol-formaldehyde resin, F127, and EOA onto the surface of plate support through pyrolysis. The adopted plate phenolic resin-based support provides strong affinity with ONCM layer. In ONCM, the larger ordered pores filling with six smaller quasi-pentagonal pores are modified by thin amorphous carbon sheets. This provides ONCM with two apparent pore size distributions and satisfactory gas separation performance. The gas permeance of resultant supported ONCM is dominated by molecular sieving mechanism. The optimum selectivity of ONCM can be reached at 46.4 (H_2/N_2), 4.7 (CO_2/N_2), and 3.3 (O_2/N_2), respectively.

ACKNOWLEDGMENTS

The authors are grateful for the financial support of this work from the National Natural Science Foundation of China (20906063), the Liaoning Natural Science Foundation of China (20102170), the Program for Liaoning Excellent Talents in University (LJQ2012010), and the State Key Laboratory of Fine Chemicals (KF1107).

REFERENCES

1. Ismail, A. F.; David, L. I. B. *J. Membr. Sci.* **2001**, *193*, 1.
2. Saufi, S. M.; Ismail, A. F. *Carbon* **2004**, *42*, 241.
3. Ash, R.; Baker, R. W.; Barer, R. W. *Procn. Roy. Soc.* **1967**, *299*, 434.
4. Koresh, J. E.; Soffer, A. *Sep. Sci. Technol.* **1983**, *18*, 723.
5. Tin, P. S.; Chung, T. S.; Hill, A. J. *Ind. Eng. Chem. Res.* **2004**, *43*, 6476.
6. Xiao, Y.; Chng, M.L.; Chung, T.-S.; Toriida, M.; Tamai, S.; Chen, H.; Jean, Y.C.J. *Carbon* **2010**, *48*, 408.
7. Tseng, H.-H.; Shiu, P.-T.; Lin, Y.-S. *Hydrogen Energy* **2011**, *36*, 15352.
8. Salleh, W. N. W.; Ismail, A. F.; Matsuura, T.; Abdullah, M. S. *Sep. Purif. Rev.* **2011**, *40*, 261.
9. Tin, P. S.; Xiao, Y.; Chung, T. S. *Sep. Purif. Rev.* **2006**, *35*, 285.
10. Wang, T.; Li, L. Spiral wound carbon membrane and preparation method thereof, UP 20110168624. 2009-7-3.

11. Kimijima, K.; Hayashi, A.; Yagi, I. *Chem. Comm.* **2008**, 5809.
12. Anderson, C. J.; Pasb, S. J.; Arora, G.; Kentish, S. E.; Hill, A. J.; Sandler, S. I.; Stevens, G. W. *J. Membr. Sci.* **2008**, *322*, 19.
13. Paul, D. R. *Science* **2012**, *335*, 413.
14. López-Lorente, A. I.; Simonet, B. M.; Valcárcel, M. *Anal. Chem.* **2010**, *82*, 5399.
15. Sholl, D. S.; Johnson. J. K. *Science* **2006**, *312*, 1003.
16. Holt, J. K.; Park, H. G.; Wang, Y.; Stadermann, M.; Artyukhin, A. B.; Grigoropoulos, C. P.; Noy, A.; Bakajin, O. *Science*, **2006**, *312*, 1034.
17. Ahn, C. H.; Baek, Y.; Lee, C.; Kim, S. O.; Kim, S.; Lee, S.; Kim, S.-H.; Bae, S. S.; Park, J.; Yoon, J. *J. Ind. Eng. Chem.* **2012**, *18*, 1551.
18. Sun, L.; Crooks, R. M. *J. Am. Chem. Soc.* **2000**, *122*, 12340.
19. Tanaka, S.; Nishiyama, N.; Egashira, Y.; Ueyama, K. *Chem. Commun.* **2005**, 2125.
20. Liang, C. D.; Hong, K. L.; Guiochon, G. A.; Mays, J. W.; Dai, S. *Angew. Chem. Int. Ed.* **2004**, *43*, 5785.
21. Zhang, F. Q.; Meng, Y.; Gu, D.; Yan, Y.; Yu, C.; Tu, B.; Zhao, D. *J. Am. Chem. Soc.* **2005**, *127*, 13508.
22. Meng, Y.; Gu, D.; Zhang, F. Q.; Shi, Y.; Yang, H.; Li, Z.; Yu, C.; Tu, B.; Zhao, D. *Angew. Chem. Int. Ed.* **2005**, *44*, 7053.
23. Simanjuntak, F. H.; Jin, J.; Nishiyama, N.; Egashira, Y.; Ueyama, K. *Carbon* **2009**, *47*, 2531.
24. Tanaka, S.; Doi, A.; Nakatani, N.; Katayama, Y.; Miyake, Y. *Carbon* **2009**, *47*, 2688.
25. Liang, C., Li, Z.; Dai, S. *Angew. Chem. Int. Ed.* **2008**, *47*, 3696.
26. Venkataraman, K.; Choate, W. T.; Torre, E. R.; Husung, R. D.; Batchu, H. R. *J. Membr. Sci.* **1988**, *39*, 259.
27. Determination of porosity of porous ceramics by density method. China National Standards GB/T 1966–1996, 1996-9-13.
28. Zhang, B.; Wang, T.; Zhang, S.; Qiu, J.; Jian, X. *Carbon* **2006**, *44*, 2764.
29. Keisha, M. S.; William, J. K. *Carbon*, **2003**, *41*, 253.
30. Mark, H.F. *Encyclopedia of Polymer Science and Technology*, Wiley. vol. 7, p 341.
31. Kim, M.; Wu, Y.; Amos, L. W. *Polymer* **1997**, *38*, 5835.
32. Zhou, W.; Yoshino, M.; Kita, H.; Okamoto, K. *Ind. Eng. Chem. Res.* **2001**, *40*, 4801.
33. Wei, W.; Qin, G.; Hu, H.; You, L.; Chen, G. *J. Membr. Sci.* **2007**, *303*, 80.
34. Lee, K. T.; Lytle, J. C.; Ergang, N. S.; Oh, S. M.; Stein, A. *Adv. Funct. Mater.* **2005**, *15*, 547.
35. Sing, K. S. W.; Everett, D. H.; Haul, R. A. W.; Mosenu, L.; Pierotti, R. A.; Rouquerol, J.; Siemieniewska, T. *Pure Appl. Chem.* **1985**, *57*, 603.
36. Jin, J.; Nishiyama, N.; Egashira, Y.; Ueyama, K. *Micropor. Mesopor. Mater.* **2009**, *118*, 218.
37. Xie, M.; Dong, H.; Zhang, D.; Guo, X.; Ding, W. *Carbon* **2011**, *49*, 2459.
38. Pang, J.; Wang, T.; Li, L.; Qi, W.; Cao, Y. *J. Inorganic Mater.* **2011**, *26*, 165. (In Chinese).
39. Tanaka, S.; Nakatani, N.; Doi, A.; Miyake, Y. *Carbon* **2011**, *49*, 3184.